J Solid State Electrochem (2011) 15:2279–2291
DOI 10.1007/s10008-011-1449-x

REVIEW

Electrochemistry and electrogenerated chemiluminescence of organic nanoparticles

Jungdon Suk · Allen J. Bard

Received: 31 March 2011 / Revised: 26 May 2011 / Accepted: 27 May 2011 / Published online: 12 July 2011

Abstract This review discusses briefly the preparation, electrochemistry, and electrogenerated chemiluminescence (ECL) as well as spectroscopic properties of organic nanoparticles. Organic nanoparticles, ranging from several tens of nanometers to hundreds of nanometers in diameter, were successfully prepared by various methods. Using a simple reprecipitation method, organic nanoparticles of a very small size can be prepared and show unique electrochemical and ECL characteristics. As with inorganic nanoparticles, organic nanoparticles suggest possible applications, like labels for the analysis of biological materials with ECL.

Keywords Electrochemistry · Electrogenerated chemiluminescence · Organic nanoparticles

Introduction

Nanoparticles are particles in the nanometer-size range, and those of a size where the properties differ from those of the bulk material are of special interest. Metal and semiconductor nanoparticles have been extensively studied and often show new physical phenomena, distinct from the bulk material, such as quantum confinement or finite size effects [1–4]. This can affect the thermal, electrical, and electronic properties. For example, the band gap (or color) of semiconductor nanoparticles in the few nanometer diameter region is a function of size and is different from that of the bulk material [5–7]. When the size of a semiconductor particle is reduced to around a 1- to 10-nm radius, the excitons (bound electron–hole pairs) are confined within the particle. This phenomenon, called the size confinement effect, has been studied by optical spectroscopy [8–12] and scanning tunneling spectroscopy [13].

As discussed below, nanoparticles of organic materials can also be synthesized and are of interest. In contrast to the extensive research that has been done on metal and inorganic semiconductor nanoparticles, the study of organic nanoparticles is still at a very early stage. The fundamental principles of the properties of organic nanoparticles are not yet well established. For many organic species, a size effect is not expected because electrons are not delocalized over nanometer domains. However, organic nanoparticles have recently received attention because of the huge range of different molecular structures, the flexibility in material synthesis and preparation, and the ability to tailor their binding affinity toward various materials [14–16]. In applications, organic nanoparticles are used as advanced materials for display elements, inks, toners, drugs, and cosmetics.

As a complement to spectroscopic methods, electrochemical ones can provide valuable insight into the size-dependent quantization effect with metal and semiconductor nanoparticles. For example, the electrochemistry of gold nanoparticles as a function of particle size has shown discrete single electron charging behavior [17–19], and there have been many studies of the electrocatalytic properties of metal nanoparticles, including those at the single particle level [20]. For semiconductor particles, when the electrochemically reduced or oxidized nanoparticles are stable, they can react with sufficient energy to form an emitting excited state and electrogenerated chemiluminescence (ECL) occurs. ECL has many advantages as an

J. Suk · A. J. Bard (✉)
Center for Electrochemistry, Department of Chemistry and Biochemistry, The University of Texas at Austin, Austin, TX 78712, USA
e-mail: ajbard@mail.utexas.edu

analytical technique compared to fluorescence, such as high sensitivity and low background. ECL has been extensively studied for organic molecules [21–23] and several semiconductor nanoparticles [24–32]. Electrochemical and ECL studies of organic nanoparticles have only recently started. A challenge in research with organic nanoparticles is controlling the particle size and shape in the same way as one can with metals and semiconductors and understanding how electrochemical and optical properties depend on size and shape. Some studies show particle-size dependence of optical constants of molecular crystals [33–35]. As discussed below, a challenge in electrochemical studies is the large size of nanoparticles currently available, resulting in small diffusion coefficients and the low concentration in aqueous solutions.

The article is arranged as follows: In "Preparation of organic nanoparticles" section, we discuss various techniques to synthesize organic nanoparticles. In "Electrochemistry and electrogenerated chemiluminescence of organic nanoparticles" section, we consider electrochemical and ECL characteristics of organic nanoparticles. These electrochemical properties of organic nanoparticles suggest possible applications. Finally, spectroscopic properties of organic nanoparticles are addressed.

Preparation of organic nanoparticles

While a large number of different approaches for the fabrication of semiconductor and metal nanoparticles have been developed, only a few techniques have been reported for the preparation of organic nanoparticles. The top-down technique of preparing nanoparticles is difficult to apply to organic materials because of their lower melting temperatures, thermal instability, and poor mechanical properties.

One approach to the preparation of sub-micrometer particles is by the mechanical milling method. The milling method is a simple and well-understood process. The size of particles obtained depends on impact and shear forces. This process has several limitations; for example, it is not appropriate for explosive, low-melting, or temperature-sensitive compounds [36]. Moreover, the processing time necessary to approach the target size can be long, and the milling agent can introduce impurities, discoloration, and fractionation. Because of aggregation during the milling process, it is difficult with this method to produce uniform organic nanoparticles having diameters smaller than 300 nm [37].

To obtain smaller nanoparticles, several methods have been developed, such as solvent deposition [38–42], laser ablation [43–45], sol–gel phase transition [46], and reprecipitation methods [47–51]. In the deposition method, organic molecules are evaporated in a vacuum chamber, and nanoscale organic aggregates are deposited on a substrate. This technique allows production of large volumes of concentrated (several milligrams per milliliter) organic nanoparticles in a single step. However, it also has drawbacks such as broad size distribution and deformation of crystal structure due to a mechanothermal effect [39, 40]. Tamaki et al. first applied the laser ablation technique to prepare organic nanoparticles from phthalocyanines and aromatic hydrocarbons [52]. These organic crystals absorb laser light, leading to a local increase in temperature and evaporation of a small fraction of material from the crystal surface [53]. Moreover, the high photon density of the laser induces surface fragmentation or cracking of the materials. A surrounding liquid helps to cool the vaporized materials rapidly and to form nanoparticles. Recently, different phthalocyanine [54], tetracene, and pentacene [55, 56] nanoparticles formed by the laser ablation technique were reported. The laser ablation technique makes more concentrated nanoparticle dispersions than other techniques and provides easy control of size and molecular packing by changing laser wavelength, pulse duration, fluence, repetition rate, irradiation period, solvent, and temperature [44, 45]. A limitation of this method is the requirement of high photon density and a narrow laser beam. Moreover, the intense laser light may cause severe photochemical damage in many organic materials.

In 1992, Kasai et al. proposed the reprecipitation method and demonstrated that nanoparticles smaller than 100 nm dispersed in water could be prepared [48]. Among the many preparation methods, this bottom-up type of technique has been widely used in nanoparticle preparation for various kinds of molecules, for example, π-conjugated organic nanocrystals [57–59], polydiacetylene derivatives [34, 60], low molecular weight aromatic compounds [61, 62], and organic functional chromophores [63–65]. The usual reprecipitation method is shown in Fig. 1. First, a target compound is dissolved at a concentration on the order of millimolars in a "good solvent" like tetrahydrofuran (THF) or alcohol (in which the compound is highly soluble). Next, a small volume (a few microliters) of this solution is injected rapidly at constant temperature into a much larger volume (~10 mL) of a vigorously stirred "poor solvent" such as water (in which the target compound is less soluble or insoluble). Smaller nanoparticles can be produced by lowering the concentration of the target compound and by reducing the volume of the injected solution. Ideally, the water should be warm (60°C), but also just below the boiling point of the good solvent, in order to make smaller nanoparticles. The key to this method is a large difference in solubilities of the target compound in the good solvent and the poor solvent and good miscibility of the two solvents. The rapid mixing of the two solvents produces a micro-environment for the target compound molecules,

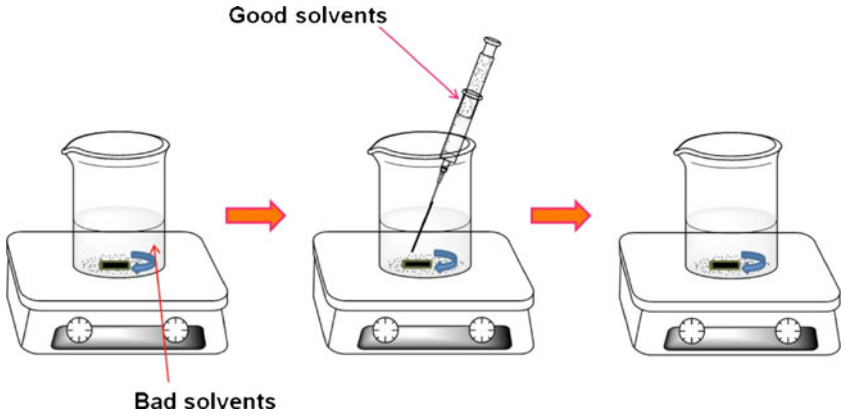

Fig. 1 Scheme of the reprecipitation method

leading to supersaturation, precipitation, and crystallization of the dispersed nanoparticles.

Unlike other preparation methods, with this process one can easily control particle size from several tens of nanometers to several micrometers. There are several variables useful in controlling the crystal size and shape in the reprecipitation process, e.g., stirring rate, injection rate, concentration of parent solution, injection volume, and temperature of the poor solvent [49]. It is, however, usually not possible with injections into water to produce particles smaller than about 20 nm. Additives, such as polymers or surfactants, can promote the formation of smaller particles. The nanoparticles formed this way can be stable from days to months. However, the presence of surfactants can have a negative effect on electrochemical reactions and the generation of ECL because the encapsulation of a particle within a layer of surfactant decreases the electron transfer rate.

Alternatively, water-soluble organic compounds such as 4′-dimethylamino-*N*-methylstilbazolum *p*-toluenesulfonate (DAST) nanoparticles are fabricated by the inverse reprecipitation method. Nanoparticles are prepared by injecting an ethanol solution of DAST into vigorously stirred decalin at room temperature. The crystal size in this case varied from about 200 to 600 nm [66, 67].

We fabricated nanoparticles dispersed in acetonitrile (MeCN) by a reprecipitation method (Suk et al., submitted for publication). Unlike many aromatic compounds, the 9-naphthylanthracene-based dimer synthesized by Wang et al. [68] is not soluble in MeCN, but is soluble in dichloromethane and THF. MeCN is one of the preferred solvents for electrochemical studies and ECL because of its wide electrochemical window. Nanoparticles were fabricated by injecting a THF solution of the 9-naphthylanthracene-based dimer into vigorously stirred MeCN (10 mL) at room temperature to produce particles as small as 16 nm. The electrochemical and ECL results are discussed below.

Electrochemistry and electrogenerated chemiluminescence of organic nanoparticles

ECL is a type of luminescence that involves the generation of oxidized and reduced species, often radical ions, at electrode surfaces that undergo a fast electron transfer reaction to produce an excited state [22, 69–71]. It is desirable in ECL to have stable and long-lived radical ions with apparent high photoluminescence (PL) quantum yield to obtain strong and bright ECL. Developing such highly efficient and stable ECL emitters over a broad spectrum of wavelength has been of interest for many years, particularly for application as an ECL label for analytical purposes, for example, for DNA determination and immunoassay [72, 73]. ECL has been extensively studied for organic molecules [22–24, 74] and a few semiconductor nanoparticles [25–28]. In commercial applications, the ECL label has largely been $Ru(bpy)_3^{2+}$ because of its good solubility in water and high ECL efficiency. One driving force in the study of organic nanoparticles, which can also be used in aqueous solution, is the possibility that, if optimized, they may find application in practical assays. The electrochemical and emission properties of organic nanoparticles have been the subject of relatively few studies compared to inorganic nanoparticles. Organic molecules have the advantage of being easily functionalized by versatile synthetic strategies, possibly tailoring the electronic and optical properties of organic nanoparticles [75]. Organic nanoparticles have the potential for many practical applications by expanding the broad spectrum of wavelengths available in ECL. ECL can be generated by annihilation (electron transfer between) the parent radical ions or by reaction of the radical with a coreactant. A coreactant is a compound that can produce a strong oxidizing or reducing agent using a reaction that follows the electrochemical electron transfer reaction. The coreactant must be energetic enough to oxidize or reduce radical ions of luminophores to produce their excited states. Typical coreactants for oxidation are tri-*n*-propylamine

(TPrA) and oxalate ion ($C_2O_4^{2-}$) and those for reduction are benzoyl peroxide and peroxydisulfate ($S_2O_8^{2-}$). Each coreactant has different potentials to produce oxidant or reductant. Depending on the electrochemical properties of the studied compound in organic solvent, a suitable coreactant can be chosen to oxidize or reduce the more stable radical ion.

Conjugated polymer nanoparticles

Organic conjugated molecules are highly fluorescent materials and are used for photo- or electroluminescent devices [76], e.g., light-emitting displays [77–79] and photovoltaics [80–83]. They are easily synthesized and can be polyfunctionalized, which allow their optical, electronic, and chemical properties to be tailored [84–86]. The first reports of colloidal dispersions of nanoparticles of conjugated polymers appeared in the 1980s, motivated by the difficult processing of conjugated polymers due to intractability and insolubility in organic solvents [87]. Conjugated polymer nanoparticles were studied in the preparation of nanoscale multiphase films for photovoltaics or for biomolecule labeling and sensing due to the high intensity and photostability of fluorescent nanoparticles as compared to conventional dyes [88, 89]. Our group has studied the electrochemical oxidation [90] and ECL [91] of nanoparticles of a conjugated copolymer, poly(9,9-dioctylfluorene-co-benzothiadiazole) (F8BT; Fig. 2). By the reprecipitation method, produced F8BT nanoparticles with a size of 25±15 nm. F8BT nanoparticles were immobilized on an ITO working electrode in an electrochemical cell (Fig. 3a) with a gold counter electrode and a silver quasireference electrode. F8BT showed electrochemically irreversible oxidation (Fig. 3b). As shown in Fig. 3c, ECL emission was produced when the potential was scanned from 0 to + 1.8 V to oxidize both F8BT nanoparticles and the coreactant, TPrA, which generates a strong reducing agent. The nanoparticle luminescence intensity increased sharply as the potential reached +1.8 V. This was the first ECL observed result from sub-25 nm single nanoparticles [92]. Studies of the electrochemistry of single immobilized particles were tracked by observing the loss of fluorescence on oxidation [91].

Aromatic hydrocarbon nanoparticles

Aromatic hydrocarbons have been widely used in ECL and solid-state electroluminescence studies. Several new anthracene derivatives have been developed and studied to tune their photophysical properties, so that new derivatives show good color purity, high efficiency, and good stability. ECL from nanoparticles of aromatic hydrocarbon compounds such as rubrene, 9,10-diphenylanthracene (DPA), and 9-naphthylanthracene-based dimer (NA) have been reported in an aqueous solution. Rubrene, DPA [92], and NA (Suk et al., submitted for publication) compounds (Fig. 2) dissolved

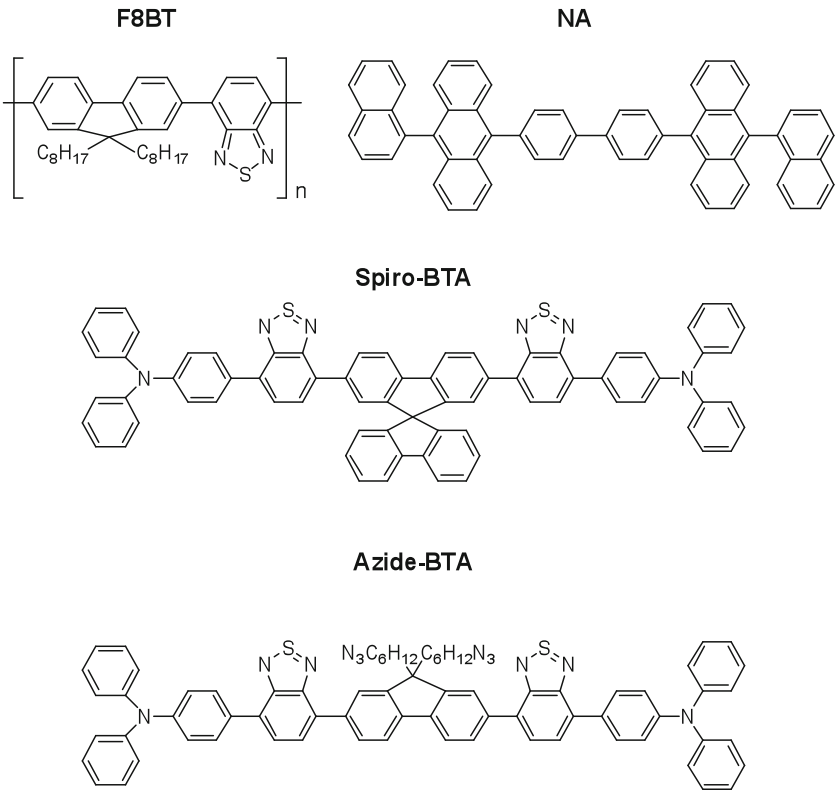

Fig. 2 Formulas of organic nanoparticles used in ECL studies

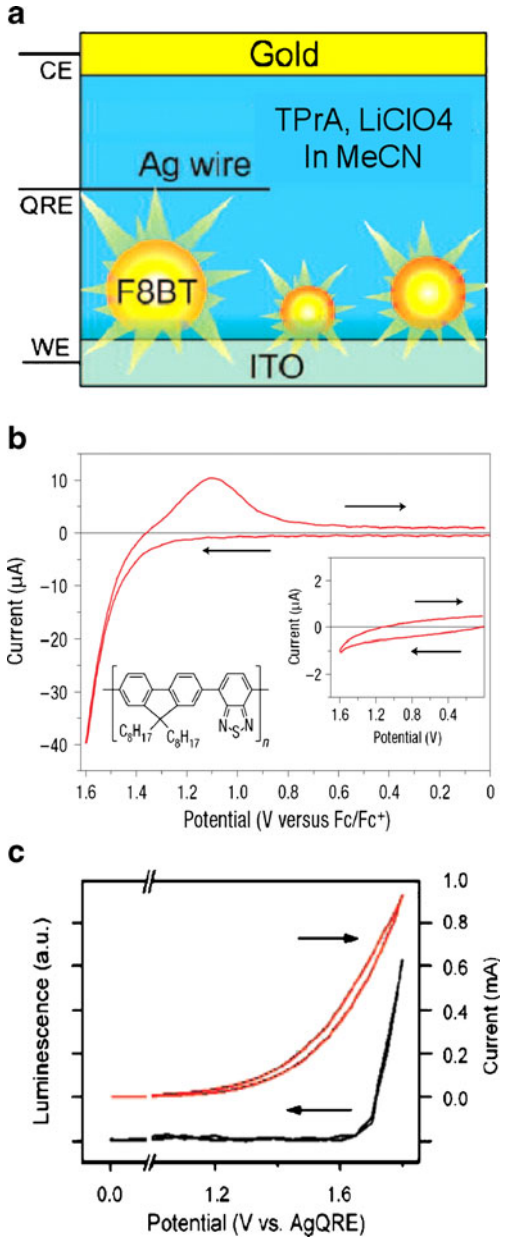

Fig. 3 **a** Schematic diagram of single molecule spectroelectrochemistry (SMS-EC) cell. *CE* counter electrode, *QRE* quasireference electrode, *WE* working electrode. **b** Cyclic voltammogram of F8BT in Nafion thin film on ITO in 0.2 M $LiClO_4$/acetonitrile solution at potential scan rate of 0.1 V/s. *Right inset* cyclic voltammogram of a Nafion film showing very small background currents over the scanned range. **c** Ensemble average of single nanoparticle ECL intensity (*black curve*) with 0.1 M TPrA and its corresponding voltammogram (*red curve*) [90, 91]

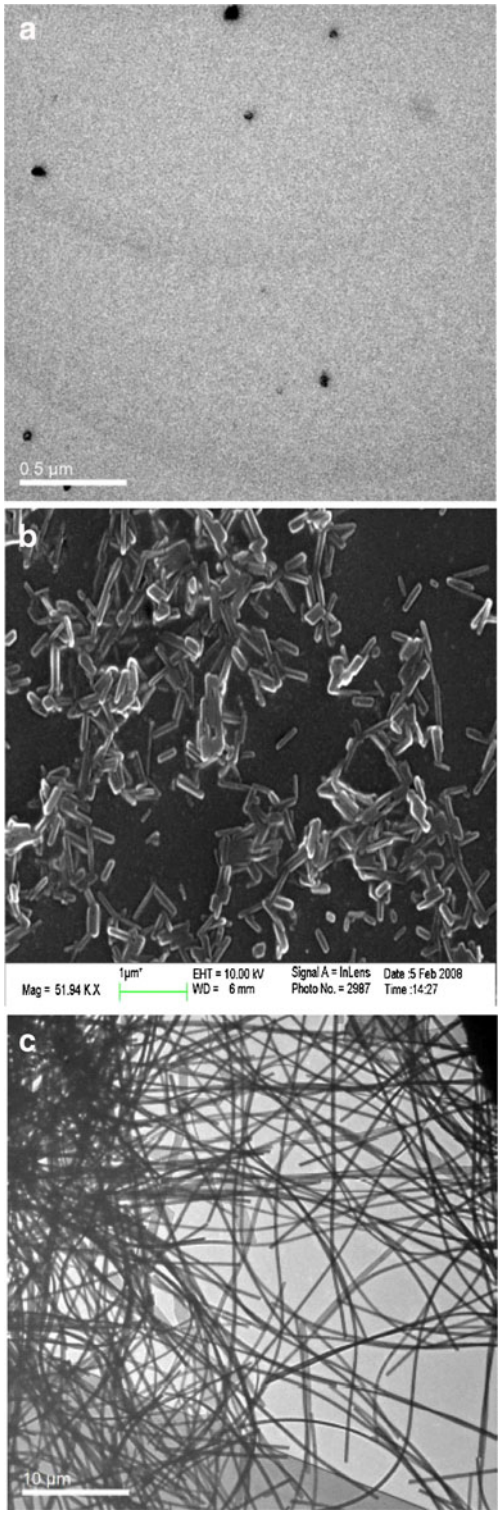

Fig. 4 **a** TEM image of freshly prepared rubrene NPs dispersed in water. **b** SEM image of DPA NPs (fresh sample). **c** TEM image of nanowires of DPA (after 1-week aging in solution) [99]

in organic solvents have been widely studied electrochemically, spectroscopically, and by ECL. They show good reversibility in electrochemistry and ECL by an annihilation reaction in organic solvent produces strong light.

Figure 4 shows the TEM image of rubrene nanoparticles and the SEM image of DPA nanoparticles after they were dispersed in water. Both nanoparticles in aqueous solution were prepared by a simple reprecipitation method, in which a small amount of an organic compound in a good solvent such as THF and MeCN was injected rapidly and stirred

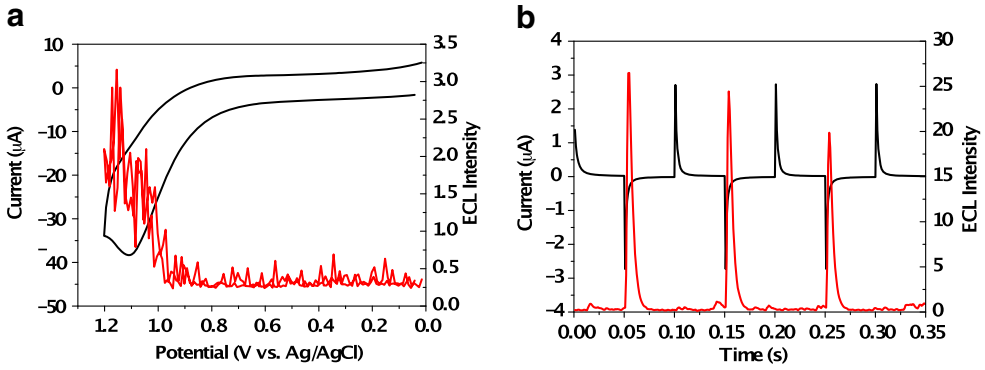

Fig. 5 **a** Cyclic voltammogram of rubrene NPs (prepared from THF) in aqueous 0.1 M $NaClO_4$ with 0.1 M TPrA at a scan rate of 500 mV/s. **b** Chronoamperometry (*black line*) and ECL transient (*red line*) of rubrene NPs, pulse width 0.1 s. *WE* Pt disk, *CE* Pt coil, *RE* Ag/AgCl. Reprinted from [99]

vigorously in a poor solvent, water. The sizes of rubrene nanoparticles determined from TEM images and dynamic light scattering measurement were ~50 nm. In the dark, rubrene nanoparticles were stable for a month without any surfactants. However, DPA nanoparticles were initially formed as nanorods (50 nm in diameter and 500 nm in length, Fig. 4b) that converted into large nanowires, about 1 μm in diameter and 10 μm in length (Fig. 4c). Although surfactants such as Triton X-100 and cetyltrimethyl ammonium bromide helped to decrease the size and avoid the formation of aggregates because of the encapsulation by the surfactants, electron transfer to the particles was hindered and this limited the generation of ECL.

Because of the limited potential window in aqueous solution and low concentration of nanoparticles, the distinctive features that could be clearly assigned to either the oxidation or reduction of the nanoparticles themselves (rather than the coreactant, TPrA) could not be distinguished. Moreover, the small diffusion coefficients of these rather large nanoparticles also result in small electrochemical signals. However, emission that can be attributed to the ECL can be observed by reaction with TPrA (Fig. 5a). Nanoparticles in the presence of a coreactant such as TPrA [93–97] or oxalate ion showed redox behavior and strong ECL light. As shown in Fig. 5a, the ECL emission was produced when the potential was scanned from 0 to +1.2 V to oxidize both rubrene nanoparticles and TPrA, which generates a strong reducing agent. Transient ECL generated from the reaction of oxidized nanoparticles and the energetic intermediates of TPrA was obtained by stepping the electrode potential with different pulse widths from 0.0 to +1.1 V versus Ag/AgCl (Fig. 5b). ECL emission was produced when the electrode potential was stepped to +1.1 V to oxidize both nanoparticles and TPrA, and no ECL was seen when the potential was stepped back to 0.0 V. The ECL signal intensity was not stable with time because of the instability of the oxidized nanoparticles in water. In the case of rubrene nanoparticles prepared from dimethylformamide (DMF), the ECL intensity was weaker; this can be attributed to the bigger particles produced because of some miscibility of the solvents with water during the reprecipitation process [98]. The ECL intensity was not strong enough to record the ECL spectrum with a CCD camera. The low concentration and diffusion coefficient of the nanoparticles and possible reactions between reducing agent and water or oxygen could explain the very low intensity of the ECL signal [99].

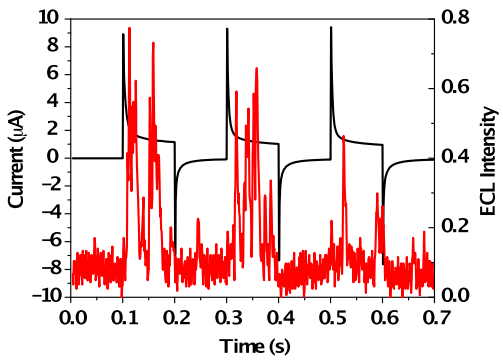

Fig. 6 Transient ECL experiment, electrochemical current (*black line*) and ECL intensity (*red line*) for DPA NPs (prepared from THF) in aqueous 0.1 M $NaClO_4$ with 0.1 M $Na_2C_2O_4$, sampling time 1 ms, pulsing pattern 0 to 1.5 V, pulse width is 0.1 s. Reprinted from [99]

In the case of DPA nanoparticles, transient ECL generated from the reaction of oxidized nanoparticles and the energetic intermediate, $CO_2^{\bullet-}$, from oxalate ion oxidation was obtained by stepping the electrode potential with different pulse widths from 0.0 to +1.5 V versus Ag/AgCl (Fig. 6). TPrA is not energetic enough to generate the excited state of DPA, so a stronger reducing agent ($CO_2^{\bullet-}$) was used to oxidize the DPA nanoparticles [100]. Due to the very small diffusion coefficients of the nanoparticles, the ECL intensity was weak.

The 9-naphthylanthracene-based dimer (NA, Fig. 2) synthesized by Wang's group has poor solubility in organic solvents such as MeCN, benzene, DMF and dimethyl sulfoxide. Among them, MeCN is a preferred solvent in ECL studies because of its wide electrochemical window to observe electrochemically generated radical cations and anions. NA nanoparticles can be prepared by a reprecipitation method, in which a small amount of NA in a good solvent (THF) is injected rapidly and stirred vigorously into

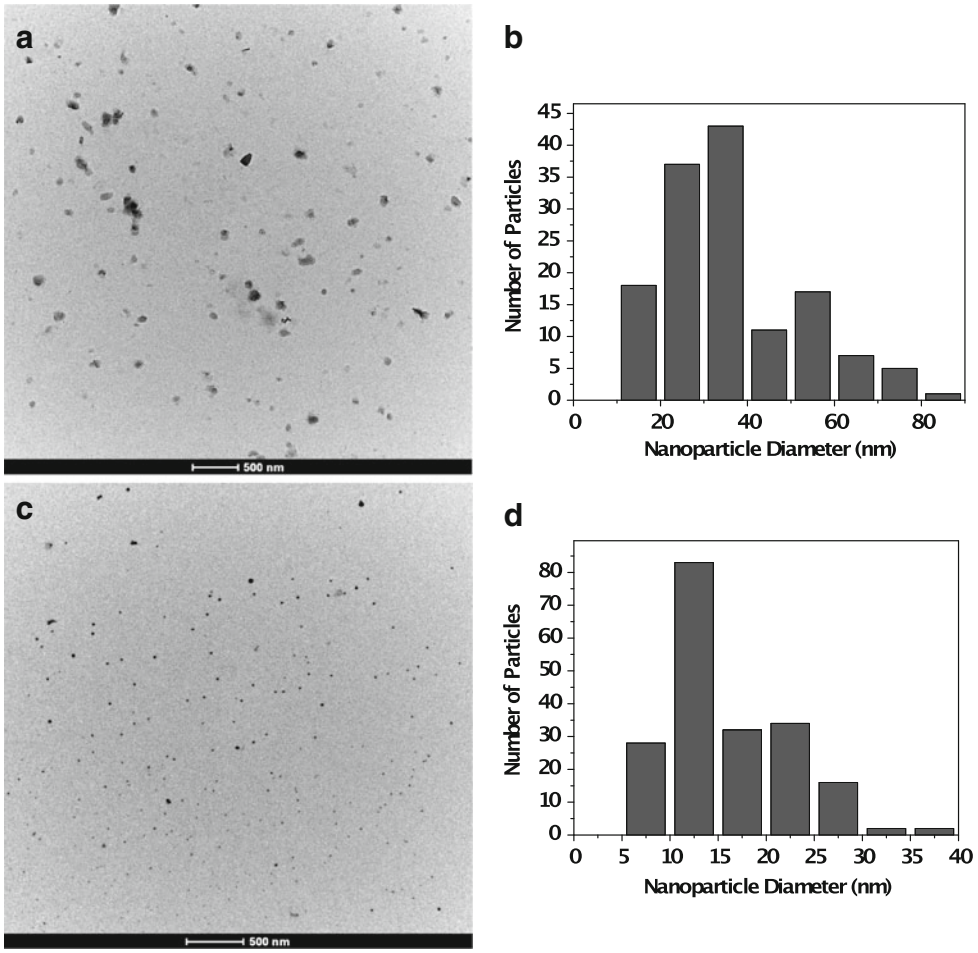

Fig. 7 **a** TEM Image of organic nanoparticles of NA dispersed in water and **b** histogram of size distribution of NA nanoparticles. The average size of the NA nanoparticles was 40±15 nm. **c** TEM image of organic nanoparticles of NA dispersed in MeCN and **d** histogram of size distribution of NA nanoparticles. The average size of NA nanoparticles was 15± 6 nm (Suk et al., in preparation)

a poor solvent (either water or MeCN). Figure 7 shows the TEM image of NA nanoparticles dispersed in both water and MeCN. Because of the different miscibility of THF with water and with MeCN, the size of NA nanoparticles obtained was different. NA nanoparticles prepared in water are significantly larger, ~40 nm, and had a less spherical shape than those in MeCN. They were stable for only a few days. On the other hand, NA nanoparticles dispersed in MeCN produced spherical, small, and well-dispersed nanoparticles. CVs of the NA nanoparticles dispersed in aqueous 0.1 M $NaClO_4$ displayed no distinctive peaks, and no ECL emission was observed because of the limited potential window in water, low concentration of nanoparticles and small diffusion coefficients (due to their large radii). However, CVs of the NA nanoparticles dispersed in MeCN are different. There is a distinctive peak at around −1.8 V, which is similar to the potential region where reduction of the NA molecule in THF occurs. Weak but noticeable ECL

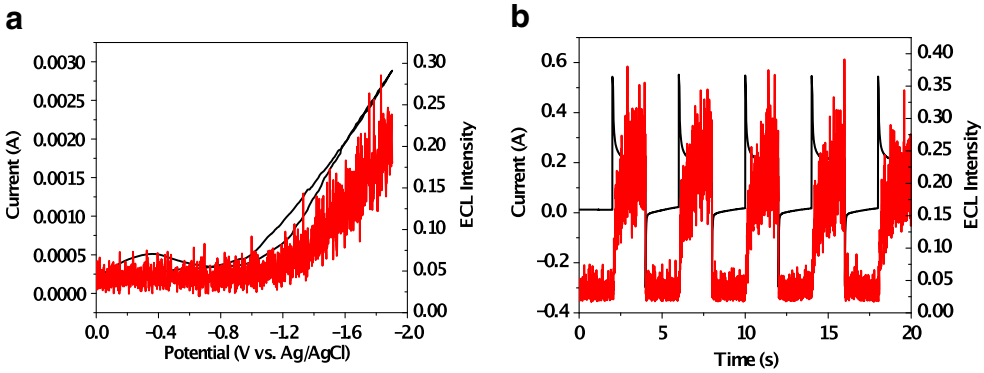

Fig. 8 **a** Cyclic voltammogram (*black line*) and ECL intensity (*red line*) of NA nanoparticles in water with 0.1 M $NaClO_4/S_2O_8^{2-}$ at scan rate of 50 mV/s and **b** transient ECL experiment, electrochemical current (*black line*) and ECL intensity (*red line*) for NA nanoparticles in water. Sampling time 1 ms, pulsing pattern 0 to −1.8 V. Pulse width is 2 s (Suk et al., in preparation)

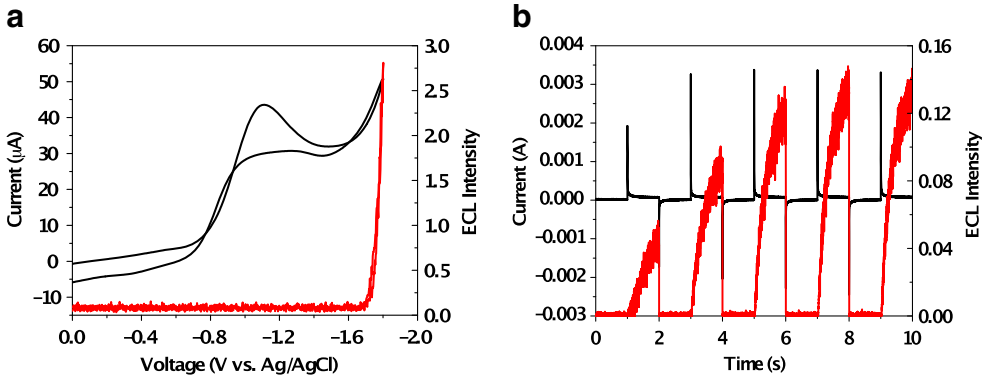

Fig. 9 **a** Cyclic voltammogram (*black line*) and ECL intensity (*red line*) of NA nanoparticles in MeCN with 0.1 M $TBAPF_6/S_2O_8^{2-}$ at scan rate of 100 mV/s and **b** transient ECL experiment, electrochemical current (*black line*) and ECL intensity (*red line*) for NA nanoparticles in MeCN with 0.1 M $TBAPF_6/S_2O_8^{2-}$. Sampling time 1 ms, pulsing pattern 0 to −1.7 V. Pulse width is 1 s (Suk et al., in preparation)

emission from the annihilation reaction was produced when the potential was scanned first toward negative and then positive potentials.

We can get information about the redox behavior and the ECL emission with a coreactant in both water and MeCN. In the case of NA nanoparticles dispersed in water, a much stronger ECL signal was observed (Fig. 8a) when the potential was scanned from 0 to −1.8 V in 0.1 M $NaClO_4$ containing 0.1 M $K_2S_2O_8$, (a coreactant which forms a strong oxidizing agent, $SO_4^{\bullet-}$) ($E_{red} \geq 3.15$ V vs. SCE) [101]. Moreover, strong ECL emission was produced by pulsing between 0 and −1.8 V. The intensity was stable with time but not strong enough to obtain an ECL spectrum (Fig. 8b). A strong ECL signal was produced with NA nanoparticles dispersed in MeCN when the potential was scanned from 0 to −1.8 V in 0.1 M MeCN containing 0.1 M $S_2O_8^-$ as a coreactant (Fig. 9a). As shown in Fig. 9b, strong ECL emission was produced when the electrode potential was stepped to −1.7 V to reduce both nanoparticles and $S_2O_8^-$. The increasing ECL signal on cycling perhaps indicates adsorption with formation of an emitting film, although there is no evidence of electrode fouling. The ECL signal was strong enough to obtain an ECL spectrum (Fig. 10, red line). The ECL spectrum of nanoparticles dispersed in MeCN showed a blue emission peak at wavelength of ~430 nm, which is close to the ECL peak of NA molecules dissolved in THF (Fig. 8, black line).

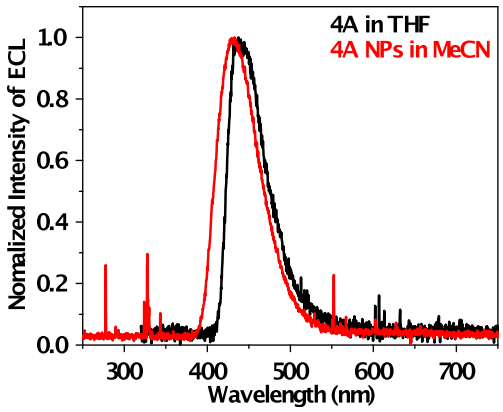

Fig. 10 ECL spectra of NA molecules in THF with 0.1 M $TBAPF_6/S_2O_8^{2-}$ (*black line*) and NA nanoparticles in MeCN with 0.1 M $TBAPF_6/S_2O_8^{2-}$ (*red line*) [Suk et al., submitted for publication]

Nanoparticles of C2-symmetric donor–acceptor compounds

ECL from nanoparticles of the recently synthesized fluorescent molecules spiro-BTA [102] and azide-BTA (Suk et al., manuscript submitted) (Fig. 2) has also been observed. Both compounds are donor–acceptor (DA) compounds that show a single reversible reduction wave ($E^o_{red} = -1.48$ V vs. SCE) and two reversible oxidation waves ($E^o_{1,ox} = 0.9$ V, $E^o_{2,ox} = 1.34$V vs. SCE) and produce red emission with a high PL quantum yield. There have been a number of studies of the electrochemical, spectroscopic, and ECL behavior of DA molecules in solution [103–108].

Spiro-BTA is a C2-symmetric compound, consisting of spirobifluorene as a π-bridge core connected to two 2,1,3-benzothiadiazole (BTA) units, the acceptors (A), and end-capped with triphenylamines as the donors (D), with an overall structure D–A–π–A–D. A reprecipitation method was used to prepare well-dispersed organic nanoparticles of the spiro-BTA in aqueous solution. Spiro-BTA nanoparticles were synthesized by injecting 100 μL of spiro-BTA in THF into 10 mL of deionized water under sonication at room temperature. Figure 11 shows the

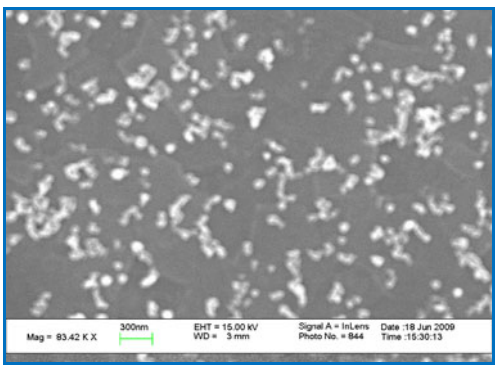

Fig. 11 SEM image of organic nanoparticles of Spiro-BTA prepared in water. Scale marker is 300 nm [102]

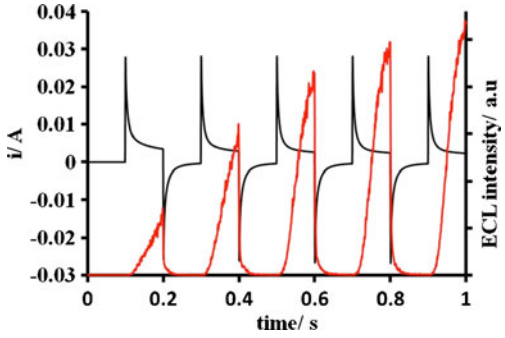

Fig. 12 *i–t* ECL of Spiro-BTA nanoparticles in water with 0.1 M TPrA as a coreactant, pulsing 0.0 to +1.2 V vs. Ag/AgCl [102]

SEM image of fresh spiro-BTA nanoparticles dispersed in water with an average diameter of ~130 nm. The particle size was stable for 1 week under ambient conditions without any surfactants.

Like other aromatic compound nanoparticles dispersed in water, there were no distinctive features that could be clearly assigned to either oxidation or reduction of nanoparticles because of the limited potential window in aqueous solutions. No ECL emission from an annihilation reaction was produced. However, with a coreactant, TPrA, ECL was obtained from well-dispersed spiro-BTA nanoparticles in an aqueous medium, as shown in Fig. 12. The ECL emission was produced when the electrode potential was stepped to +1.2 V to oxidize both nanoparticles and TPrA, and no ECL was produced when the electrode potential was stepped back to 0.0 V. The ECL signal was moderate and increased, like the result of NA nanoparticles dispersed in MeCN with $S_2O_8^-$. The increasing ECL signal on cycling might be from the formation of an emitting film, but again in this case there was no evidence of electrode fouling.

Azide-BTA is also a C2-symmetric DA compound, consisting of two 2,1,3-BTA groups as the acceptors and triphenylamine as the donors bridged by a fluorene moiety. A reprecipitation method was used to synthesize these nanoparticles. Figure 13 shows the TEM image of well-dispersed and spherical nanoparticles with an average diameter of 16 nm produced by reprecipitation in water; these are the smallest nanoparticles produced so far by the reprecipitation technique. The size distribution indicates that the measured diameters range from a few to 40 nm. The very small size of the nanoparticles was controlled by the preparation conditions, e.g., concentration of azide-BTA in THF, water temperature, stirring rate, and dropping method into water. The production of small nanoparticles with a narrow size distribution is important to increase the diffusion coefficients. However, CVs of dispersed azide-BTA nanoparticles in water with 0.1 M $NaClO_4$ displayed no distinctive peaks in the oxidation and reduction region. ECL emission from the annihilation reaction was produced when the potential was first scanned negative and then positive (Fig. 14a). The transient ECL generated from annihilation is weakly observed when the electrode potential is stepped from −2.2 to + 2.3 V versus Ag/AgCl (Fig. 14b). ECL emission was stable with time, but the light intensity was not strong enough to obtain a spectrum. Even though the size of nanoparticles was small, low concentration and small diffusion coefficient of nanoparticles allowed only a weak light intensity.

Unlike Spiro-BTA, TPrA was not a good coreactant for azide-BTA. However, the oxidation of azide-BTA nanoparticles in the presence of oxalate ions produced ECL by a potential sweep or step (Fig. 14c, d). A much stronger ECL signal was observed when the potential was scanned from 0 to −1.8 V in 0.1 M $NaClO_4$ containing 0.1 M $K_2S_2O_8$ (a coreactant that forms a strong oxidizing agent) (Fig. 12e). Moreover, pulsing between 0 and −1.8 V produced strong ECL emission. The intensity was stable with time and strong enough to obtain an ECL spectrum (Fig. 14f). The ECL spectrum (Fig. 15, red dotted line) of nanoparticles showed a red emission peak at a wavelength of ~670 nm,

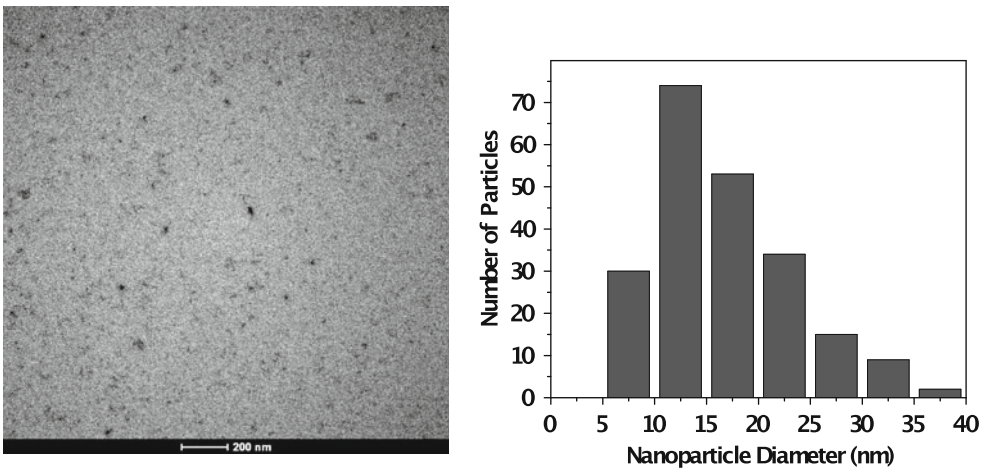

Fig. 13 *Left* TEM image of organic nanoparticles of azide-BTA dispersed in water. *Right* histogram of size distribution. The average size of azide-BTA nanoparticles is 16±5 nm (Suk et al., in preparation)

which is close to the ECL peak of azide-BTA molecules (Fig. 15, red solid line). The strong and broad ECL spectrum (with ~200-nm half width) from nanoparticles seems to consist of multiple peaks due to the various sizes of the nanoparticles. This is the first ECL spectrum from organic nanoparticles dispersed in water.

Spectroscopic properties of organic nanoparticles

Unlike metal and inorganic semiconductor nanoparticles, which show typical nanometer-size dependence, the spectroscopy of organic nanoparticles has been the subject of relatively few studies. Only several cases of size-dependent optical properties in molecular crystals have been reported [33, 36, 109–111]. Only some organic nanoparticles such as perylene [35, 112], phthalocyanine [112, 113], and pyrazoline nanoparticles [114] have shown size effects in the absorption and fluorescence spectra, the latter attributed to fluorescence emission enhancement because of conformational changes of the molecules [114, 115]. In the perylene system, a blue shift in the absorption band maximum of about 30 nm was observed on a decreasing particle size from 200 to 50 nm [112]. A blue shift of the absorption maximum by about 15 nm was also found with decreasing particle size from 150 to 70 nm [35]. The fluorescence spectra of various sizes of organic nanoparticles can exhibit a similar result. However, a study of these phenomena to explain and define a confinement effect suffers from the current limitation in preparing particles smaller than ~20 nm. Intra- and intermolecular effects by fluorophore aggregation might induce these phenomena [116–119]. The intramolecular effect depends on conformational changes of the fluorophores. For example, nanoparticles made by

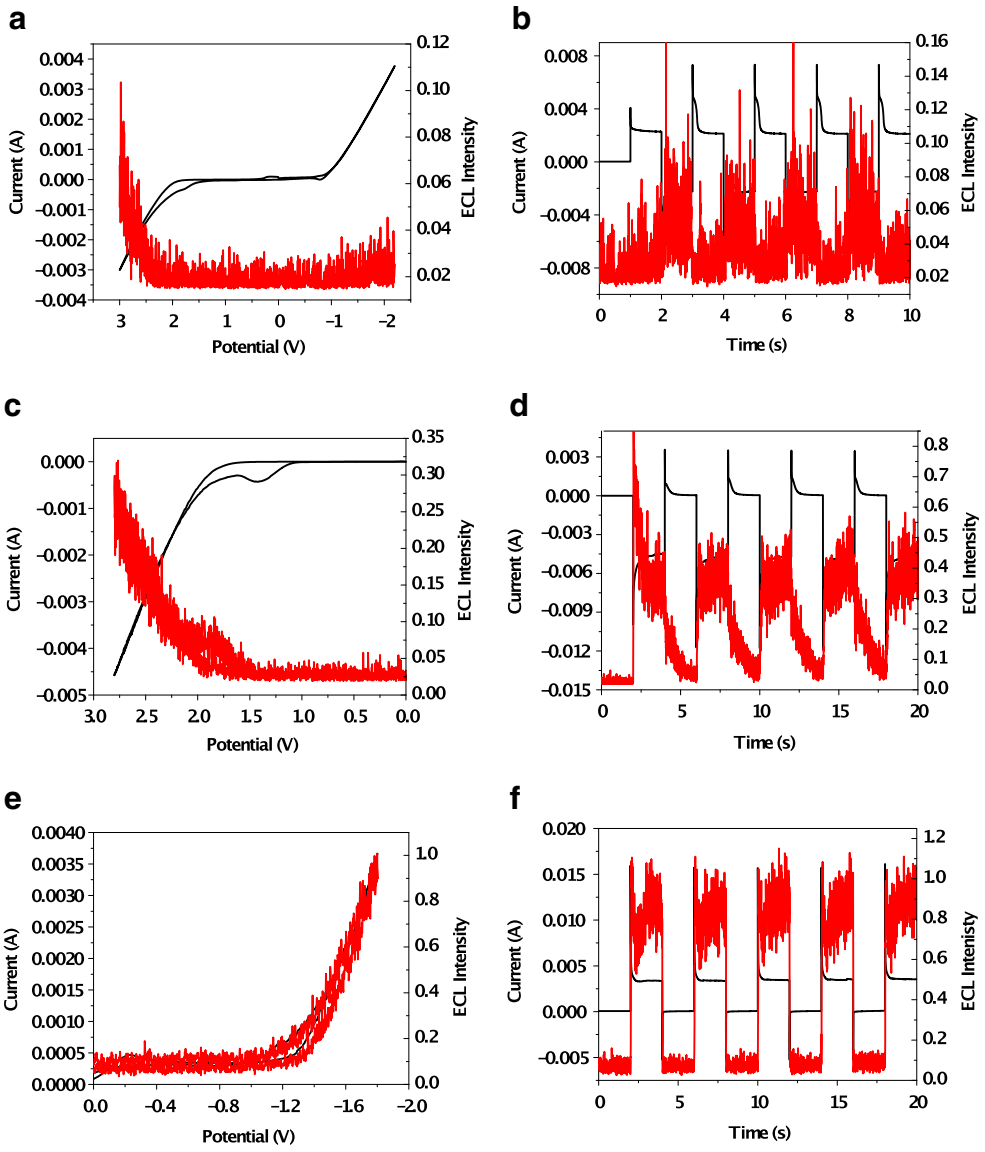

Fig. 14 **a** Cyclic voltammogram (*black line*) and ECL intensity (*red line*) of azide-BTA nanoparticles in water with 0.1 M $NaClO_4$ at a scan rate of 100 mV/s. **b** Transient ECL experiment, electrochemical current (*black line*) and ECL intensity (*red line*) for azide-BTA nanoparticles in water with 0.1 M $NaClO_4$. Sampling time 1 ms, pulsing pattern: from −2 to 2.7 V, pulse width is 1 s. **c** CV of azide-BTA nanoparticles in aqueous 0.1 M $NaClO_4$ with 0.1 M oxalate. **d** Transient ECL experiment for azide-BTA nanoparticles with 0.1 M oxalate, sampling time 1 ms, pulsing pattern 0 to 2.5 V, pulse width is 2 s. **e** CV of azide-BTA nanoparticles in aqueous 0.1 M $NaClO_4$ with 0.1 M peroxy disulfate. **f** Transient ECL experiment for azide-BTA nanoparticles with 0.1 M peroxy disulfate, sampling time 1 ms, pulsing pattern 0 to −1.8 V, pulse width is 2 s. *WE* Pt disk, *CE* Pt coil, *RE* Ag/AgCl (Suk et al., in preparation)

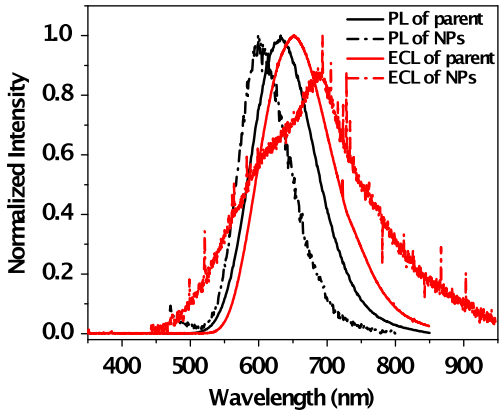

Fig. 15 Fluorescence (*black*) and ECL (*red*) spectra of azide-BTA solution and nanoparticles. *Solid line* azide-BTA parent solution in 1:1 Bz/MeCN, *dotted line* azide-BTA nanoparticles dispersed in water. Slit width 0.75 mm, integration time 5 min for ECL of parent solution, 10 min for ECL of nanoparticles (Suk et al., in preparation)

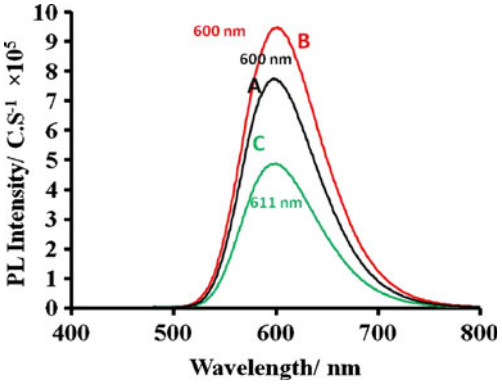

Fig. 17 Emission spectra: *A black* fresh Spiro-BTA nanoparticles; *B red* nanoparticles with Triton X-100 in water; *C green* 100 μL of 1 mM Spiro-BTA in 10 mL THF [99]

oligophenylenevinylenes with a series of substituents showed fluorescence enhancement by intramolecular twisting, which suppresses the radiation process [120]. Intermolecular effects are correlated with aggregates such as H- and J-aggregates. In the absorption case, the transition of an H-aggregate (card-stack structure) [121, 122] from the ground state to a lower coupled excited state is forbidden [123]. As a result, the absorption of the H-aggregate appears blue-shifted [124]. In this case, emission of the H-aggregate is quenched because the internal conversion from a higher electronic state to a lower electronic state is faster than emission. For the J-aggregate structure, the molecules are arranged in head-to-tail direction. This structure induces a red-shifted absorption and stronger fluorescence than that of the monomer because the transition from the ground state to a lower coupled excited state is allowed [125, 126]. Figure 16 shows a comparison of absorption spectra of different β-carotene formulations that have different aggregate structures and particle sizes [127]. The absorption spectrum of the amorphous nanoparticles showed an increasing blue shift with decreasing particle size, whereas a red shift with change in band structure characterizes the spectra of the crystalline dispersion colloids.

The nanoparticles of aromatic hydrocarbon compounds such as rubrene, DPA, and NA and one of C2-symmetric DA compounds, azide-BTA, showed little difference in the absorption and emission spectra of nanoparticles compared with the molecules dissolved in an organic solvent and showed little effect of size with no enhancement of fluorescence intensity or efficiency. However, the spectroscopy of spiro-BTA is different. The emission of spiro-BTA nanoparticles is blue-shifted by 10 nm as compared to that of spiro-BTA in THF. Moreover, the PL intensity of spiro-BTA nanoparticles with surfactant was larger than for spiro-BTA in THF (Fig. 17). The blue-shifted emission is ascribed to the restricted conformational relaxation in these nanoparticles, which also leads to enhancement of emission intensity as reported for aggregation-induced emission enhancement [128].

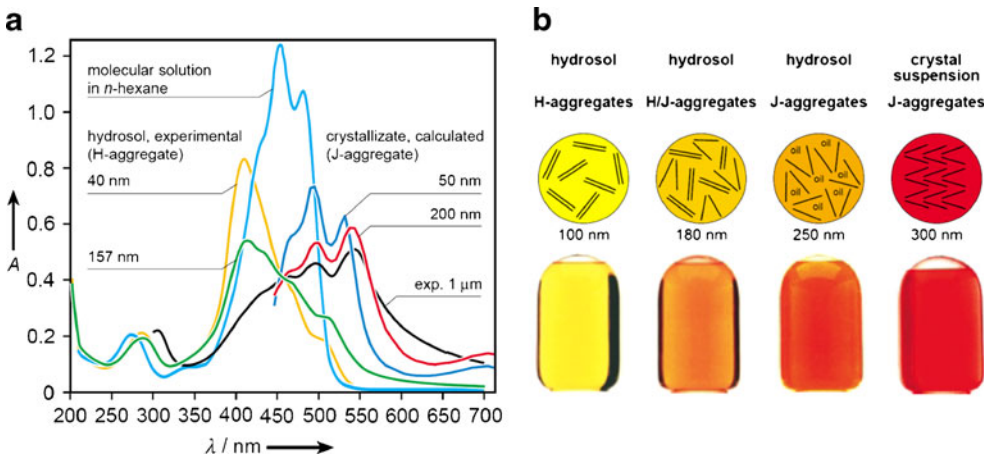

Fig. 16 **a** UV/Vis absorption spectra of 5 ppm β-carotene. Influence of aggregate structure and particle size compared with the molecular solution in *n*-hexane. **b** Influence of particle size and aggregation structure on the color tone nuance of nanodispersed β-carotene hydrosols [127]

Summary and outlook

In this article, we have tried to provide a perspective about the possibility of studying organic nanoparticles electrochemically and by ECL. Currently, the research based on organic nanoparticles and nanomaterials is still in its infancy and much remains to be done in this area. Size-dependent optical and electronic properties have not been elucidated completely, due to limitations of synthesizing very small nanoparticles in significant quantities. New approaches are needed for the preparation of monodisperse nanoparticles of controlled size. Studies of the effect of surface modification are also needed. If suitable stable and efficient nanoparticles can be found, applications like labels for biological material analysis by ECL would be possible.

Acknowledgments We acknowledge the support of this research from Roche Diagnostics, Inc. and the Robert A. Welch Foundation (F-0021).

References

1. Kubo R, Kawabata A, Kobayashi S (1984) Annu Rev Mater Sci 14:49
2. Rossetti R, Ellison JL, Gibson JM, Brus LE (1984) J Chem Phys 80:4464
3. Hanamura E (1988) Phys Rev B: Condens Matter 38:1228
4. Medintz IL, Uyeda HT, Goldman ER, Mattoussi H (2005) Nat Mater 4:435
5. Alivisatos AP (1996) Science 271:933
6. Guzelian AA, Katari JEB, Kadavanich AV, Banin U, Hamad K, Juban E, Alivisatos AP, Wolters RH, Arnold CC, Heath JR (1996) J Phys Chem 100:7212
7. Trindade T, O'Brien P, Pickett NL (2001) Chem Mater 13:3843
8. Mittleman DM, Schoenlein RW, Shiang JJ, Colvin VL, Alivisatos AP, Shank CV (1994) Phys Rev B: Condens Matter 49:14435
9. de Paula AM, Barbosa LC, Cruz CHB, Alves OL, Sanjurjo JA, Cesar CL (1996) Appl Phys Lett 69:357
10. Freire PTC, Silva MAA, Reynoso VCS, Vaz AR, Lemos V (1997) Phys Rev B: Condens Matter 55:6743
11. Carbone L, Nobile C, De Giorgi M, Sala FD, Morello G, Pompa P, Hytch M, Snoeck E, Fiore A, Franchini IR, Nadasan M, Silvestre AF, Chiodo L, Kudera S, Cingolani R, Krahne R, Manna L (2007) Nano Lett 7:2942
12. Dzhagan V, Valakh MY, Kolny-Olesiak J, Lokteva I, Zahn DRT (2009) Appl Phys Lett 94:243101
13. Jdira L, Liljeroth P, Stoffels E, Vanmaekelbergh D, Speller S (2006) Phys Rev B: Condens Matter 73:115305
14. Peng AD, Xiao DB, Ma Y, Yang WS, Yao JN (2005) Adv Mater 17:2070
15. Patra A, Hebalkar N, Sreedhar B, Sarkar M, Samanta A, Radhakrishnan TR (2006) Small 2:650
16. Kaeser A, Schenning APHJ (2010) Adv Mater 22:2985
17. Chen SW, Murray RW, Feldberg SW (1998) J Phys Chem B 102:9898
18. Hicks JF, Zamborini FP, Osisek A, Murray RW (2001) J Am Chem Soc 123:7048
19. Hicks JF, Miles DT, Murray RW (2002) J Am Chem Soc 124:13322
20. Bard AJ, Zhou HJ, Kwon SJ (2010) Is J Chem 50:267
21. Bard AJ (ed) (2004) Electrogenerated chemiluminescence. Marcel Dekker, New York
22. Richter MM (2004) Chem Rev 104:3003
23. Miao WJ (2008) Chem Rev 108:2506
24. Ding ZF, Quinn BM, Haram SK, Pell LE, Korgel BA, Bard AJ (2002) Science 296:1293
25. Myung N, Ding ZF, Bard AJ (2002) Nano Lett 2:1315
26. Myung N, Bae Y, Bard AJ (2003) Nano Lett 3:1053
27. Bae Y, Myung N, Bard AJ (2004) Nano Lett 4:1153
28. Myung N, Lu XM, Johnston KP, Bard AJ (2004) Nano Lett 4:183
29. Bard AJ, Ding ZF, Myung N (2005) Struct Bond 118:1
30. Ren T, Xu JZ, Tu YF, Xu S, Zhu JJ (2005) Electrochem Commun 7:5
31. Chen M, Pan LJ, Huang ZQ, Cao JM, Zheng YD, Zhan HQ (2007) Mater Chem Phys 101:317
32. Shen LH, Cui XX, Qi HL, Zhang CX (2007) J Phys Chem C 111:8172
33. Horn D, Honigmann B (1974) XII FATIPEC Kongress. Verlag Chemie, Weinheim, p 181
34. Katagi H, Kasai H, Okada S, Oikawa H, Komatsu K, Matsuda H, Liu ZF, Nakanishi H (1996) Jpn J Appl Phys Part 2 35:L1364
35. Katagi H, Kasai H, Okada S, Oikawa H, Matsuda H, Nakanishi H (1997) J Macromol Sci Pure Appl Chem A34:2013
36. Texter J (2001) J Dispers Sci Technol 22:499
37. Rabinow BE (2004) Nat Rev Drug Discov 3:785
38. Seko T, Ogura K, Kawakami Y, Sugino H, Toyotama H, Tanaka J (1998) Chem Phys Lett 291:438
39. Balzer F, Bordo VG, Simonsen AC, Rubahn HG (2003) Appl Phys Lett 82:10
40. Liu HB, Li YL, Xiao SQ, Gan HY, Jiu TG, Li HM, Jiang L, Zhu DB, Yu DP, Xiang B, Chen YF (2003) J Am Chem Soc 125:10794
41. Chiu JJ, Kei CC, Perng TP, Wang WS (2003) Adv Mater 15:1361
42. Ong BS, Wu YL, Liu P, Gardner S (2004) J Am Chem Soc 126:3378
43. Tamaki Y, Asahi T, Masuhara H (2002) J Phys Chem A 106:2135
44. Tamaki Y, Asahi T, Masuhara H (2003) Jpn J Appl Phys Part 1 42:2725
45. Asahi T, Sugiyama T, Masuhara H (2008) Acc Chem Res 41:1790
46. Ibanez A, Maximov S, Guin A, Chaillout C, Baldeck PL (1998) Adv Mater 10:1540
47. Kasai H, Nalwa HS, Oikawa H, Okada S, Matsuda H, Minami N, Kakuta A, Ono K, Mukoh A, Nakanishi H (1992) Jpn J Appl Phys Part 2 31:L1132
48. Kasai H, Oikawa H, Okada S, Nakanishi H (1998) Bull Chem Soc Jpn 71:2597
49. Wu CF, Peng HS, Jiang YF, McNeill J (2006) J Phys Chem B 110:14148
50. Kaneko Y, Shimadai S, Onodera T, Kimura T, Matsuda H, Okada S, Kasai H, Oikawa H, Kakudate Y, Nakanishi H (2007) Jpn J Appl Phys Part 1 46:6893
51. Mori J, Miyashita Y, Oliveira D, Kasai H, Oikawa H, Nakanishi H (2009) J Cryst Growth 311:553
52. Tamaki Y, Ashshi T, Masuhara H (2000) Appl Surf Sci 168:85
53. Kostler S, Rudorfer A, Haase A, Satzinger V, Jakopic G, Ribitsch V (2009) Adv Mater 21:2505
54. Masuhara H, Ashahi T (2003) Single organic nanoparticles. Springer, Berlin, p 32
55. Kita S, Masuo S, Machida S, Itaya A (2006) Jpn J Appl Phys Part 1 45:6501
56. Kostler S, Rudorfer A, Berghauser R, Jakopic G, Ribitsch V (2006) Adv Materi Forum Iii, Pts 1 and 2 514–516:1235
57. Nalwa HS, Kasai H, Okada S, Oikawa H, Matsuda H, Kakuta A, Mukoh A, Nakanishi H (1993) Adv Mater 5:758

58. Grey JK, Kim DY, Norris BC, Miller WL, Barbara PF (2006) J Phys Chem B 110:25568
59. Cui S, Liu HB, Gan LB, Li YL, Zhu DB (2008) Adv Mater 20:2918
60. Matsuda H, Yamada S, VanKeuren E, Katagi H, Kasai H, Okada S, Oikawa H, Nakanishi H, Smith EC, Kar AK, Wherrett BS (1997) Photosensit Opt Mater Devices 2998:241
61. Kim HY, Bjorklund TG, Lim SH, Bardeen CJ (2003) Langmuir 19:3941
62. Oliveira D, Baba K, Mori J, Miyashita Y, Kasai H, Oikawa H, Nakanishi H (2010) J Cryst Growth 312:431
63. Kasai H, Kamatani H, Yoshikawa Y, Okada S, Oikawa H, Watanabe A, Itoh O, Nakanishi H (1997) Chem Lett 1181
64. Gesquiere AJ, Uwada T, Asahi T, Masuhara H, Barbara PF (2005) Nano Lett 5:1321
65. Olive AGL, Del Guerzo A, Schafer C, Belin C, Raffy G, Giansante C (2010) J Phys Chem C 114:10410
66. Oikawa H, Fujita S, Kasai H, Okada S, Tripathy SK, Nakanishi H (2000) Colloids Surf A 169:251
67. Okazoe S, Fujita S, Kasai H, Okada S, Oikawa H, Nakanishi H (2001) Mol Cryst Liq Cryst 367:11
68. Wang L, Wong WY, Lin MF, Wong WK, Cheah KW, Tam HL, Chen CH (2008) J Mater Chem 18:4529
69. Faulkner LR, Bard AJ (1977) In: Bard AJ (ed) Electroanalytical chemistry, vol 10. Dekker, New York, pp 1–95
70. Faulkner LR, Glass RS (1982) In: Waldemar A, Giuseppe C (eds) Chemical and biological generation of excited states. New York, Academic, Chapter 6
71. Bard AJ, Debad JD, Leland JK, Sigal GB, Wilbur JL, Wohlstadter JN (2002) In: Meyers RA (ed) Encyclopedia of analytical chemistry: applications, theory and instrumentation, vol 11. Wiley, New York, p 9842
72. Namba Y, Sawada T, Suzuki O (2000) Anal Sci 16:757
73. Cao WD, Ferrance JP, Demas J, Landers JP (2006) J Am Chem Soc 128:7572
74. Knight AW, Greenway GM (1994) Analyst 119:879
75. Balazs AC, Emrick T, Russell TP (2006) Science 314:1107
76. Burroughes JH, Bradley DDC, Brown AR, Marks RN, Mackay K, Friend RH, Burns PL, Holmes AB (1990) Nature 347:539
77. Grimsdale AC, Chan KL, Martin RE, Jokisz PG, Holmes AB (2009) Chem Rev 109:897
78. Mullen K, Scherf U (2005) Organic light-emitting devices. Wiley-VCH, Weinheim
79. Nalwa HS, Rohwer LS (2003) Handbook of luminescence display materials and devices. American Scientific, Stevenson Ranch
80. Scharber MC, Wuhlbacher D, Koppe M, Denk P, Waldauf C, Heeger AJ, Brabec CL (2006) Adv Mater 18:789
81. Chen JW, Cao Y (2009) Acc Chem Res 42:1709
82. Peet J, Heeger AJ, Bazan GC (2009) Acc Chem Res 42:1700
83. Cheng YJ, Yang SH, Hsu CS (2009) Chem Rev 109:5868
84. Hoeben FJM, Jonkheijm P, Meijer EW, Schenning APHJ (2005) Chem Rev 105:1491
85. Yamamoto Y, Fukushima T, Suna Y, Ishii N, Saeki A, Seki S, Tagawa S, Taniguchi M, Kawai T, Aida T (2006) Science 314:1761
86. Grimsdale AC, Mullen K (2005) Angew Chem Int Ed 44:5592
87. Gunes S, Neugebauer H, Sariciftci NS (2007) Chem Rev 107:1324
88. Chan WCW, Nie SM (1998) Science 281:2016
89. Bruchez M, Moronne M, Gin P, Weiss S, Alivisatos AP (1998) Science 281:2013
90. Palacios RE, Fan FRF, Grey JK, Suk J, Bard AJ, Barbara PF (2007) Nat Mater 6:680
91. Chang YL, Palacios RE, Fan FRF, Bard AJ, Barbara PF (2008) J Am Chem Soc 130:8906
92. Maloy JT, Bard AJ (1971) J Am Chem Soc 93:5968
93. Smith JH, Mann CK (1969) J Org Chem 34:1821
94. Noffsinger JB, Danielson ND (1987) Anal Chem 59:865
95. Zu YB, Bard AJ (2000) Anal Chem 72:3223
96. Kanoufi F, Cannes C, Zu YB, Bard AJ (2001) J Phys Chem B 105:8951
97. Miao WJ, Choi JP, Bard AJ (2002) J Am Chem Soc 124:14478
98. Chung HR, Kwon E, Kawa H, Kasai H, Nakanishi H (2006) J Cryst Growth 294:459
99. Omer KM, Bard AJ (2009) J Phys Chem C 113:11575
100. Lai RY, Bard AJ (2003) J Phys Chem A 107:3335
101. Memming R (1969) J Electrochem Soc 116:785
102. Omer KM, Ku SY, Cheng JZ, Chou SH, Wong KT, Bard AJ (2011) J Am Chem Soc 133:5492–5499
103. Fungo F, Wong KT, Ku SY, Hung YY, Bard AJ (2005) J Phys Chem B 109:3984
104. Rashidnadimi S, Hung TH, Wong KT, Bard AJ (2008) J Am Chem Soc 130:634
105. Omer KM, Ku SY, Wong KT, Bard AJ (2009) Angew Chem Int Ed 48:9300
106. Omer KM, Ku SY, Wong KT, Bard AJ (2009) J Am Chem Soc 131:10733
107. Shen M, Rodriguez-Lopez J, Lee YT, Chen CT, Fan FRF, Bard AJ (2010) J Phys Chem C 114:9772
108. Omer KM, Ku SY, Chen YC, Wong KT, Bard AJ (2010) J Am Chem Soc 132:10944
109. Kasai H, Kamatani H, Okada S, Oikawa H, Matsuda H, Nakanishi H (1996) Jpn J Appl Phys Part 2 35:L221
110. Fu HB, Ji XH, Zhang XH, Wu SK, Yao JN (1999) J Colloid Interface Sci 220:177
111. Fu HB, Yao JN (2001) J Am Chem Soc 123:1434
112. Kasai H, Yoshikawa Y, Seko T, Okada S, Oikawa H, Mastuda H, Watanabe A, Ito O, Toyotama H, Nakanishi H (1997) Mol Cryst Liq Cryst Sci Technol Sect A 294:173
113. Komai Y, Kasai H, Hirakoso H, Hakuta Y, Okada S, Oikawa H, Adschiri T, Inomata H, Arai K, Nakanishi H (1998) Mol Cryst Liq Cryst Sci Technol Sect A 322:167
114. An BK, Kwon SK, Jung SD, Park SY (2002) J Am Chem Soc 124:14410
115. Feng X, Tong B, Shen J, Shi J, Han T, Chen L, Zhi J, Lu P, Ma Y, Dong Y (2010) J Phys Chem B 114:16731
116. Miteva T, Palmer L, Kloppenburg L, Neher D, Bunz UHF (2000) Macromolecules 33:652
117. Deans R, Kim J, Machacek MR, Swager TM (2000) J Am Chem Soc 122:8565
118. Luo JD, Xie ZL, Lam JWY, Cheng L, Chen HY, Qiu CF, Kwok HS, Zhan XW, Liu YQ, Zhu DB, Tang BZ (2001) Chem Commun 1740
119. Walters KA, Ley KD, Schanze KS (1999) Langmuir 15:5676
120. Oelkrug D, Tompert A, Gierschner J, Egelhaaf HJ, Hanack M, Hohloch M, Steinhuber E (1998) J Phys Chem B 102:1902
121. Kasha M, Rawls HR, El-Bayouni A (1965) Pure Appl Chem 11:371
122. Dahne L, Biller E (1998) Adv Mater 10:241
123. Li S, He L, Ziong F, Li Y, Yang G (2004) J Phys Chem B 108:10887
124. Gruszecki WI (1991) J Biol Phys 18:99
125. Akins DL, Macklin JW (1989) J Phys Chem 93:5999
126. Chowdhury A, Wachsmann-Hogiu S, Bangal PR, Raheem I, Peteanu LA (2001) J Phys Chem B 105:12196
127. Horn D, Lűddecke E (1996) In: Pelizzetti E (ed) Fine particles science and technology—from micro to nanoparticles. Kluwer, Dordrecht, p 761
128. Zeng Q, Li Z, Dong Y, Di C, Qin A, Hong Y, Ji L, Zhu Z, Jim KW, Yu G, Li Q, Li Z, Liu Y, Qin J, Tang BZ (2007) Chem Commun 1:70